nature climate change

SUPPLEMENTARY INFORMATION
https://doi.org/10.1038/s41558-018-0278-7

In the format provided by the authors and unedited.

Differential vulnerability to climate change yields novel deep-reef communities

Martin Pierre Marzloff[1,2*], Eric C. J. Oliver[1,3], Neville S. Barrett[1], Neil J. Holbrook[1,4], Lainey James[1], Simon J. Wotherspoon[1,5] and Craig R. Johnson[1]

[1]Institute for Marine and Antarctic Studies, University of Tasmania, Hobart, Tasmania, Australia. [2]Benthic and Coastal Ecology laboratory (LEBCO), DYNECO Research Unit, Ifremer, Centre de Bretagne , Plouzané, France. [3]Department of Oceanography, Dalhousie University, Halifax, Nova Scotia, Canada. [4]Australian Research Council Centre of Excellence for Climate Extremes, University of Tasmania, Hobart, Tasmania, Australia. [5]Australian Antarctic Division, Kingston, Tasmania, Australia. *e-mail: Martin.Marzloff@ifremer.fr

Supplementary information to "Differential vulnerability to climate change yields novel deep reef communities"

Martin P. Marzloff *et al.*

17 July 2018

This document provides some supplementary information related to our paper "Differential vulnerability to climate change yields novel deep reef communities". Here are provided technical details associated with the distribution models presented in our paper, structured as several distinct sections:

1. Environmental Covariates
2. Random Forest Model Fits
3. Projections of Current And 2060s Distributions
4. Projected Changes In Latitudinal Distributions
5. Additional contextual information: Autonomous Underwater Vehicle (AUV) imagery dataset, strengths and limitations of the study

1 Environmental covariates used to fit the distribution models

We extracted a range of oceanographic, biogeochemical and seafloor-related variables (see Fig. A2) to characterise the environmental conditions associated with the occurence of each functional group. These variables are plotted as maps across the study region in Fig. A2: (a) aspect, (b) depth, (c) relief and (d) slope of the seafloor were obtained from Geoscience Australia, which maps out these features at 250 m resolution [1] based on all available acoustic survey in the region.

In addition to these seafloor features (depth, relief, slope, aspect), we considered a range of environmental covariates related to biogeochemical conditions (mean salinity, nitrate concentration, and phytoplankton concentration) and sea surface temperature (SST mean, variance, skewness, minimum and maximum), for which high resolution projections through the 2060s were available [2, 3, 4]. Skewness refers to the asymmetry in daily temperature distribution around the annual mean (negative or positive values for left-skewed or right-skewed distributions, respectively).

Note that, temperature-depth profiles through the water column suggest high mixing on the continental shelf, which legitimises the use of SST as a proxy for bottom temperature. Smale and Wernberg [5] conclude that SST constitutes a valid proxy to characterise long-term climatology of bottom temperature on the continental shelf over large scales ($>$ 100 km). Stobart *et al.* [6] show a tight relationship between satellite SSTs (which strongly constrain the annual mean estimates of SST used in our study [7]) and in situ bottom temperatures in coastal Australia. Moreover, we inspected the correlation between sea surface temperature (SST) and bottom temperature on the continental shelf of eastern Australia based on available data from IMOS moorings, temperature sensors on the AUV, and benthic temperature loggers deployed around Tasmania (Craig Mundy, unpublished data). We found that some local stratification can occur between surface and bottom water parcels at fine spatio-temporal scales (e.g. seasonal stratification occurs in some places), but that overall SST constitutes a valid proxy for bottom temperature on the continental shelf over large-scales and smoothed over seasonal signals. Fig. A1 illustrates the strong consistency between annual mean bottom water temperature estimates (extrapolated from sparse observations in the CSIRO Atlas of Regional Seas 2006; http://www.marine.csiro.au/ dunn/cars2006/) and annual mean SST estimates used in our study [7]. The Pearson correlation coefficient between annual mean temperature estimates at each of the study sites using these 2 climatologies is 0.94. Note that the CARS 2006 climatology is based on extrapolation between available observations, so sparseness of data can bias local bottom water estimates (see CARS website for details). Since we used a long-term climatology of SST across a large latitudinal gradient, we are confident in the robustness of these data in the context of our study.

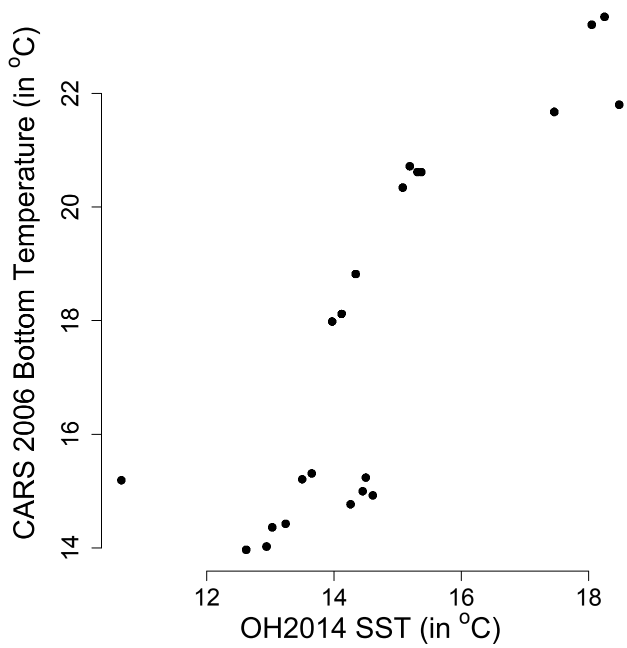

Figure A1: Comparison of mean annual temperature estimates at each of the AUV deployment sites from SST climatology versus bottom water climatology. The Pearson correlation between annual mean bottom water temperature (estimates from CSIRO Atlas of Regional Seas 2006; http://www.marine.csiro.au/ dunn/cars2006/) and annual mean Sea Surface Temperature estimates used in our study (OH 2014; Oliver and Holbrook, 2014) is 0.94

Ocean variables are derived from available 9-year time series for the 1990s and 2060s, and projections through the 2060s are based on dynamically downscaled ocean climate change projections from a coupled climate model taking account of CO_2 increases according to the IPCC AR4 "business as usual" A1B scenario [2, 3, 4]. Mean SST was further statistically downscaled to the coast [7] while the other variables were taken directly from the high-resolution ocean dynamical model [2, 3, 4]. While we do not account for the long-term effects of ocean acidification, we capture the effects of coastal ocean warming, which is expected to be a major signature of climate-driven changes in the next decades in the region [8].

(a) Aspect

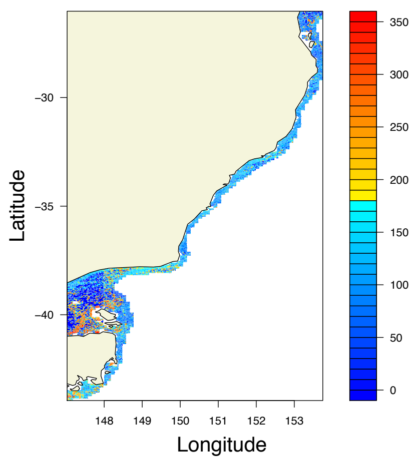

(b) Depth

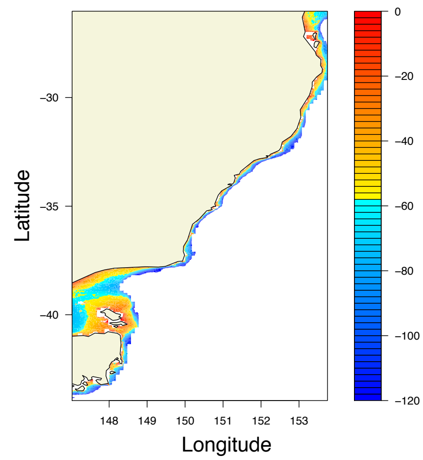

(c) Relief (log)

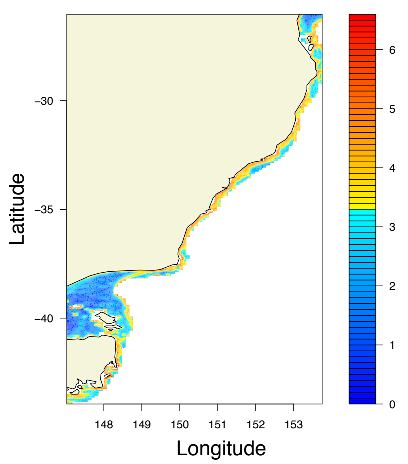

(d) Slope (log)

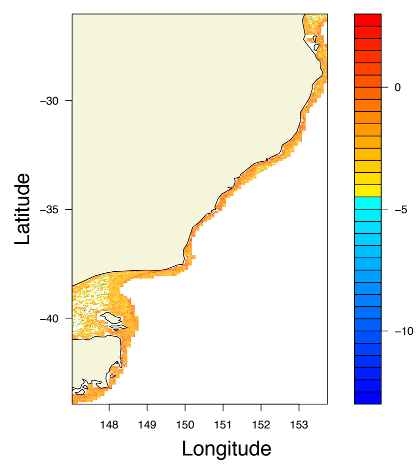

(e) NO_3 1990s concentration

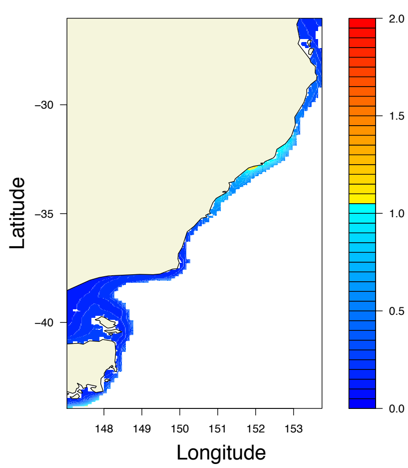

(f) NO_3 2060s concentration

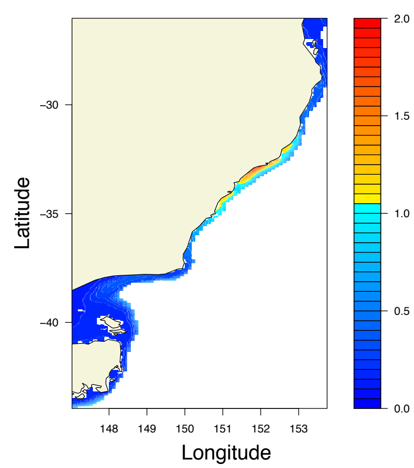

(g) 1990s primary production

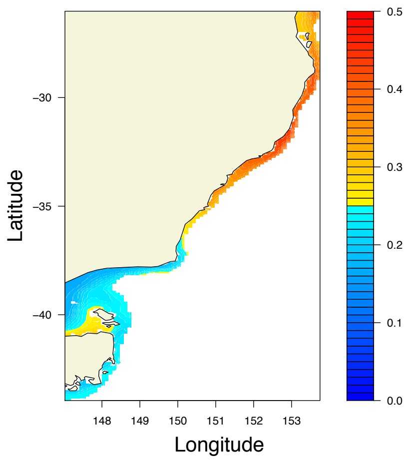

(h) 2060s primary production

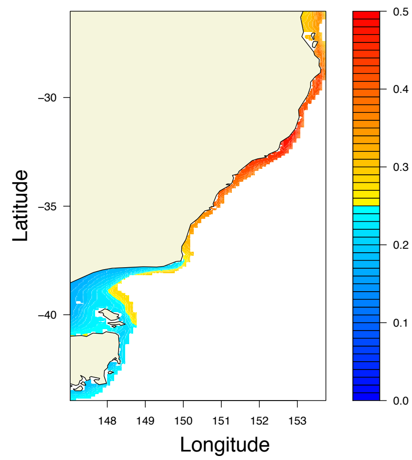

(i) Mean 1990s salinity

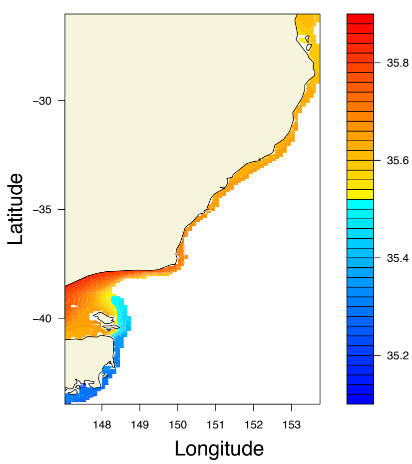

(j) Mean 2060s salinity

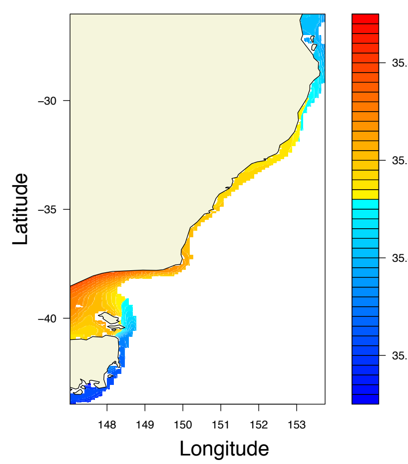

(k) Maximum 1990s SST

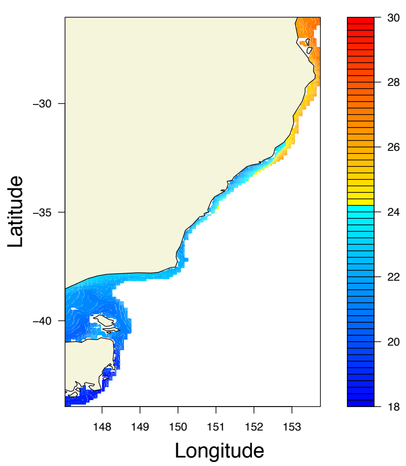

(l) Maximum 2060s SST

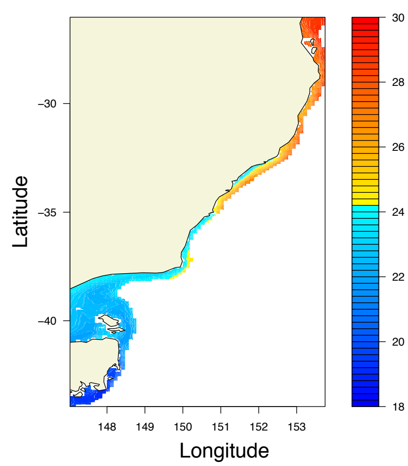

(m) Mean 1990s SST

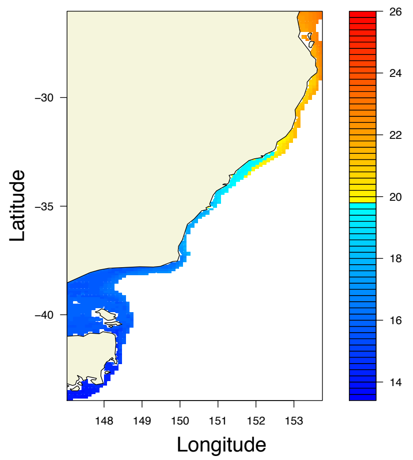

(n) Mean 2060s SST

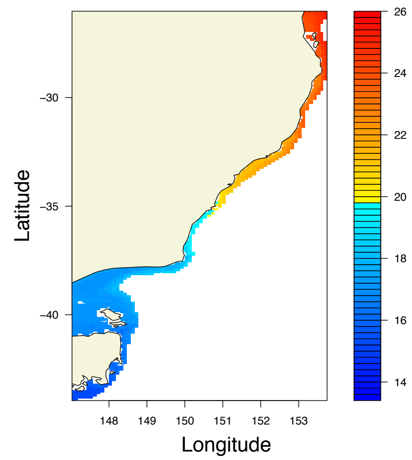

(o) Minimum 1990s SST

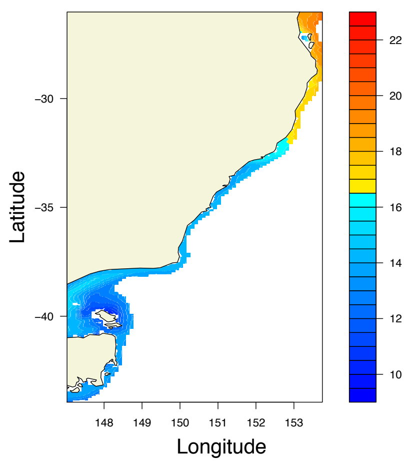

(p) Minimum 2060s SST

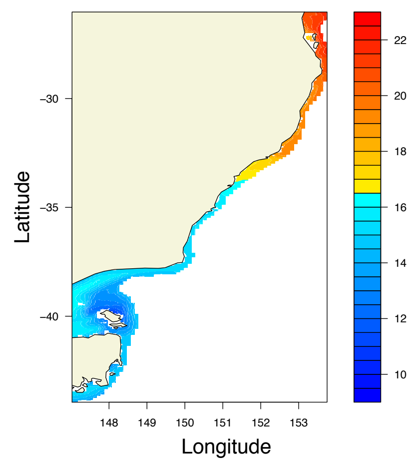

(q) 1990s skewness in SST

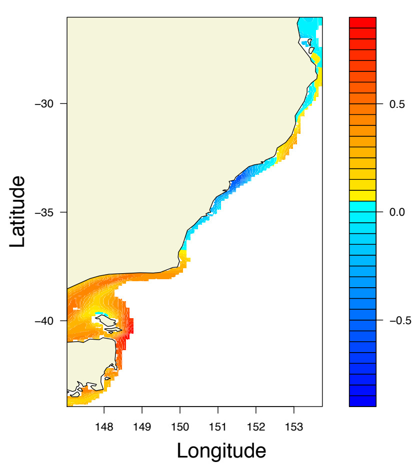

(r) 2060s skewness in SST

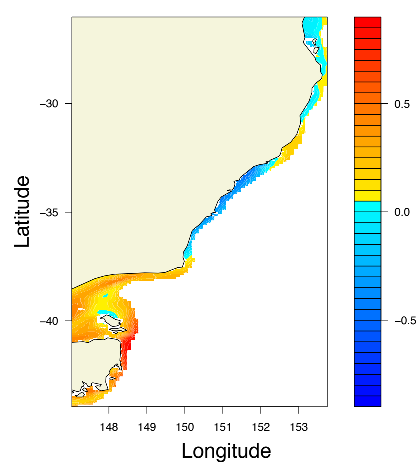

(s) 1990s variance in SST (log)

(t) 2060s variance in SST (log)

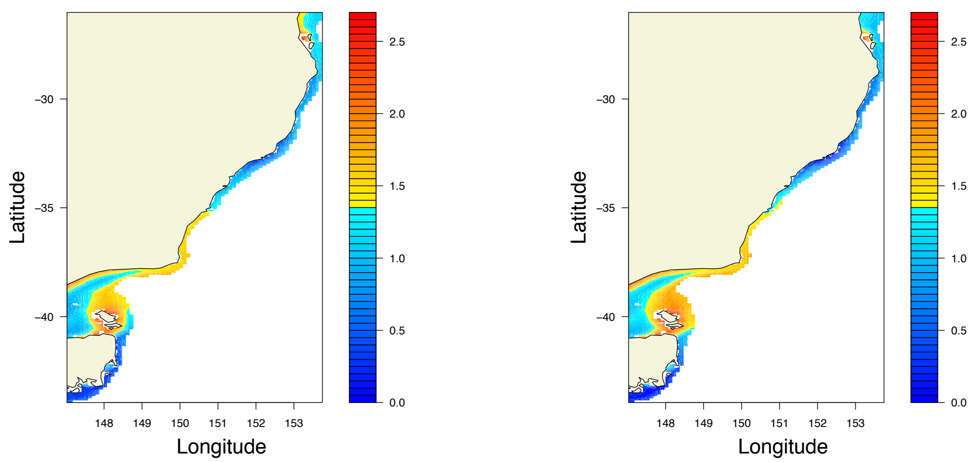

Figure A2: Maps of predictors used to determine optimal environmental conditions for each of the functional groups used in the study. Aspect of the slope is given as a compass direction in degrees; Depth in metres; NO_3 in μg/L; Primary production is approximated as annual mean chlorophyll a concentration in mg/m^3; Salinity in g/L; Sea Surface Temperature is given in $^\circ$C.

2 Random Forest Model Fits

Overall, model cross-validation error rates are good for a study of this nature. They do vary across models and highlight the limited predictability of local-scale variability for a small number of groups, but these do not compromise the robustness of our large-scale predictions about each group's biogeography. The mean misclassification error rate, which accounts for both false positives and false negatives (assessed against 'out-of-bag' samples that did not contribute to fitting individual classification trees; Breiman, 2001 [9]) was only 16% (mean across all groups) and varied from $\sim$ 2% for octocorals to $\sim$ 33% for laminar sponges (Table A1). Note that for 11 out of the 13 functional groups, out-of-bag mean misclassification error rates are inferior or equal to 20% (Table A1).

2.1 Cross-validation of the different models: Prediction Error Rates and Receiver Operating Characteristic (ROC) curve

Across all 13 functional groups, Random Forest models have Area Under the Curve (AUC) indices that qualify their performance as ranging between "excellent" ($AUC > 0.9$), e.g. for octocorals (CBBNA) or radial 'ball' sponges (SPMR), and "fair" ($0.8 > AUC > 0.7$), e.g. for hollow cup sponges (SPHC) or hollow tubular sponges (SPHT).

Random forests have "excellent" (AUC > 0.9) accuracy for 5 out of the 13 groups that have truncated distribution across the latitudinal gradient (i.e. massive sponge, rigid and soft gorgonian, octocorals and balls sponges). For 6 out of the 13 groups that are either more broadly distributed across the study area (i.e. asicidians, bryozoans, cup sponges, palmate sponges), or spatially-constrained and rare (e.g. black corals), random forests predictions are "good" (0.9> AUC> 0.8). For 3 out of the 13 groups (i.e. branching sponge, laminar sponge, tubular sponge) that are broadly distributed but whose occurrence varies at fine spatial scales and cannot be explained due to lack of high resolution environmental data, model accuracy can only be classified as "fair" (0.8> AUC >0.7). We acknowledge that classification error rate estimates based on 'out-of-bag' bootstrapped samples of the data are moderately high for certain models, but these have to be nuanced by these AUC values. Even for these broadly-distributed groups for which site-to-site variability is harder to predict, most models predict current-day latitudinal ranges of all functional groups that are consistent with available records.

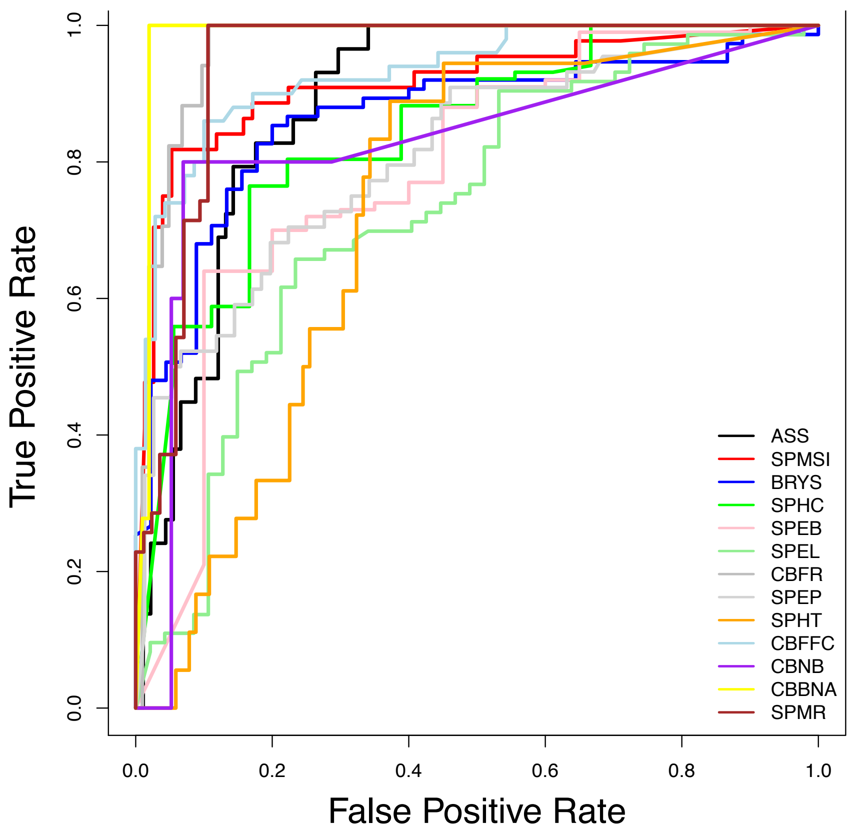

Figure A3: Accuracy of Random Forest (500 trees) fit against observed presence / absence of the 13 functional groups from 2010-2013 AUV surveys in the study region depicted as Receiver Operating Characteristic (ROC) curve characterising misclassification errors as a function of the probability threshold value chosen to discriminate between presence and absence. (Stalked Solitary Ascidians: ASS, Bryozoans: BRYS,Octocorals: CBBNA, Soft Gorgonians: CBFFC, Rigid Gorgonians: CBFR, Black Coral: CBNB, Branching Sponges: SPEB, Laminar Sponges: SPEL, Palmate Sponges: SPEP, Hollow Cup Sponges: SPHC, Hollow Tubular Sponges: SPHT, Ball or Radiate Sponges: SPMR, Massive Form Sponges: SPMSI).

As complementary pieces of information concerning model fit, we provide misclassification error rates (both false positives and false negatives) based on model cross-validation. This consists in assessing model predictions using a set threshold to classify predicted probabilities of presence into 'presence' or 'absence' and comparing against the 'out-of-bag' samples, i.e. the observations not used to fit the model. Note that even when associated with higher classification error rates (e.g. SPEL = Palmate Sponges or SPHT = hollow tubular sponges), random forest models are still useful in adequately characterising the current-day latitudinal range, i.e. the broad biogeography, of each of the 13 functional groups.

Table A1: Prediction error rates from cross-validation (OOB: out-of-bag; 0: false negatives; 1: false positives) and Area Under the Curve estimes (AUC, including standard deviation) for the Random Forest distribution model (500 trees) for the 13 functional groups (Stalked Solitary Ascidians: ASS, Bryozoans: BRYS,Octocorals: CBBNA, Soft Gorgonians: CBFFC, Rigid Gorgonians: CBFR, Black Coral: CBNB, Branching Sponges: SPEB, Laminar Sponges: SPEL, Palmate Sponges: SPEP, Hollow Cup Sponges: SPHC,Hollow Tubular Sponges: SPHT,Ball or Radiate Sponges: SPMR, Massive Form Sponges: SPMSI).

	OOB	OOB 0	OOB 1	AUC	AUC sd
ASS	0.2	0.12	0.45	0.89	0.03
SPMSI	0.13	0.11	0.18	0.92	0.03
BRYS	0.18	0.2	0.16	0.86	0.03
SPHC	0.14	0.67	0.05	0.84	0.05
SPEB	0.17	0.65	0.07	0.79	0.06
SPEL	0.33	0.47	0.25	0.73	0.05
CBFR	0.08	0.04	0.35	0.97	0.01
SPEP	0.25	0.16	0.41	0.81	0.04
SPHT	0.2	0.09	0.83	0.73	0.05
CBFFC	0.13	0.1	0.16	0.93	0.02
CBNB	0.08	0.04	1	0.83	0.12
CBBNA	0.02	0.02	0	0.98	0.01
SPMR	0.13	0.11	0.2	0.94	0.02
mean	0.16	0.21	0.32	0.86	0.04

2.1.1 Random Forest model performance for Stalked Solitary Ascidians

Table A2: Confusion matrix with prediction error rates (top: false negatives; bottom: false positives) for the Random Forest distribution model (500 trees) for Stalked Solitary Ascidians .

Prediction	True	False	Error
0	80	11	0.121
1	16	13	0.448

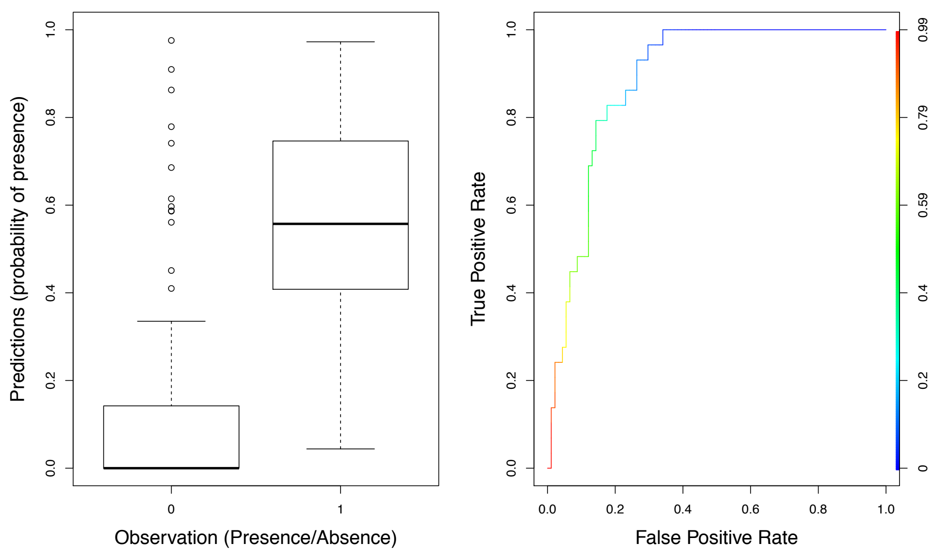

Figure A4: Accuracy of Random Forest (500 trees) fit against observed presence / absence of Stalked Solitary Ascidians from 2010-2013 AUV surveys. Box plot of predicted probability of presence against observed presence (1) / absence (0) (left-hand panel). Receiver Operating Characteristic (ROC) curve characterising misclassification errors as a function of the probability threshold value chosen to discriminate between presence and absence (right-hand panel).

2.1.2 Random Forest model performance for Bryozoans

Table A3: Confusion matrix with prediction error rates (top: false negatives; bottom: false positives) for the Random Forest distribution model (500 trees) for Bryozoans .

Prediction	True	False	Error
0	36	9	0.2
1	63	12	0.16

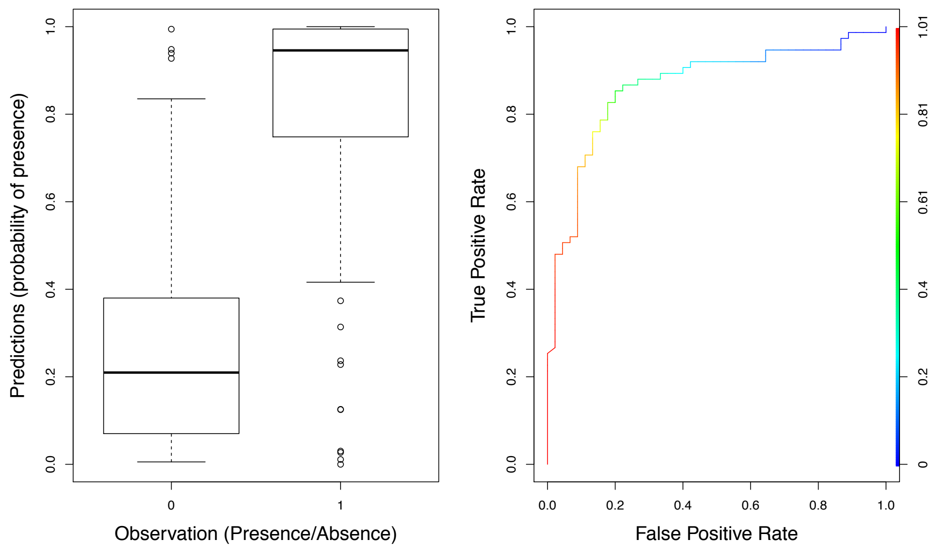

Figure A5: Accuracy of Random Forest (500 trees) fit against observed presence / absence of Bryozoans from 2010-2013 AUV surveys. Box plot of predicted probability of presence against observed presence (1) / absence (0) (left-hand panel). Receiver Operating Characteristic (ROC) curve characterising misclassification errors as a function of the probability threshold value chosen to discriminate between presence and absence (right-hand panel).

2.1.3 Random Forest model performance for Octocorals

Table A4: Confusion matrix with prediction error rates (top: false negatives; bottom: false positives) for the Random Forest distribution model (500 trees) for Octocorals .

Prediction	True	False	Error
0	100	2	0.02
1	18	0	0

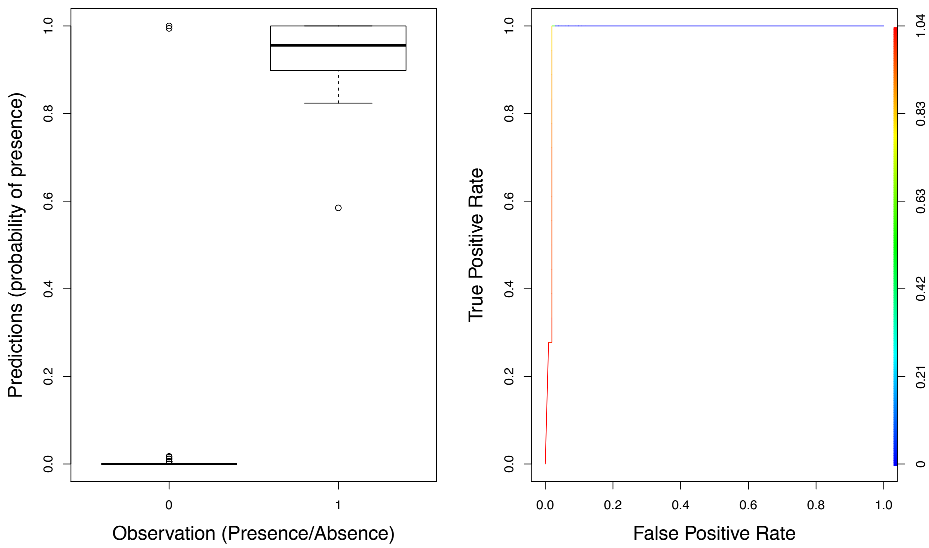

Figure A6: Accuracy of Random Forest (500 trees) fit against observed presence / absence of Octocorals from 2010-2013 AUV surveys. Box plot of predicted probability of presence against observed presence (1) / absence (0) (left-hand panel). Receiver Operating Characteristic (ROC) curve characterising misclassification errors as a function of the probability threshold value chosen to discriminate between presence and absence (right-hand panel).

2.1.4 Random Forest model performance for Soft Gorgonians

Table A5: Confusion matrix with prediction error rates (top: false negatives; bottom: false positives) for the Random Forest distribution model (500 trees) for Soft Gorgonians .

Prediction	True	False	Error
0	63	7	0.1
1	42	8	0.16

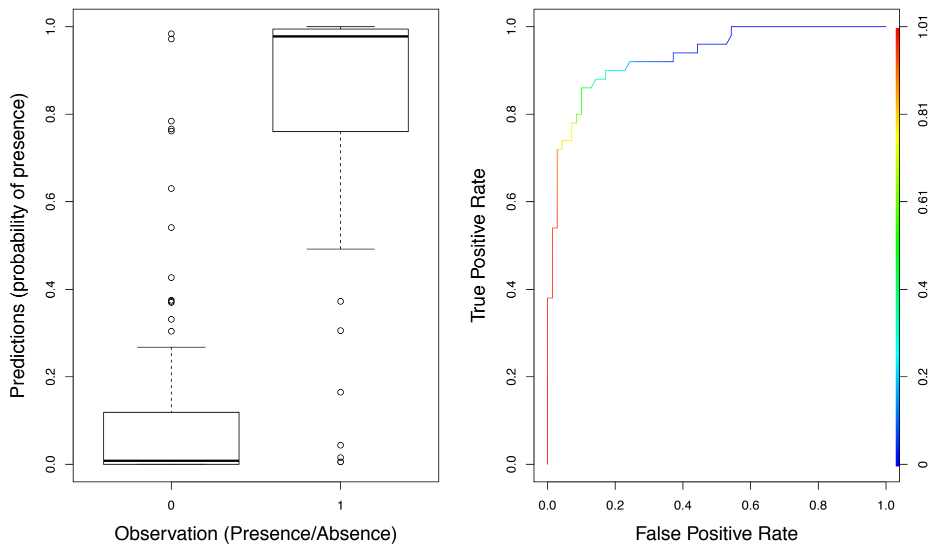

Figure A7: Accuracy of Random Forest (500 trees) fit against observed presence / absence of Soft Gorgonians from 2010-2013 AUV surveys. Box plot of predicted probability of presence against observed presence (1) / absence (0) (left-hand panel). Receiver Operating Characteristic (ROC) curve characterising misclassification errors as a function of the probability threshold value chosen to discriminate between presence and absence (right-hand panel).

2.1.5 Random Forest model performance for Rigid Gorgonians

Table A6: Confusion matrix with prediction error rates (top: false negatives; bottom: false positives) for the Random Forest distribution model (500 trees) for Rigid Gorgonians .

Prediction	True	False	Error
0	99	4	0.039
1	11	6	0.353

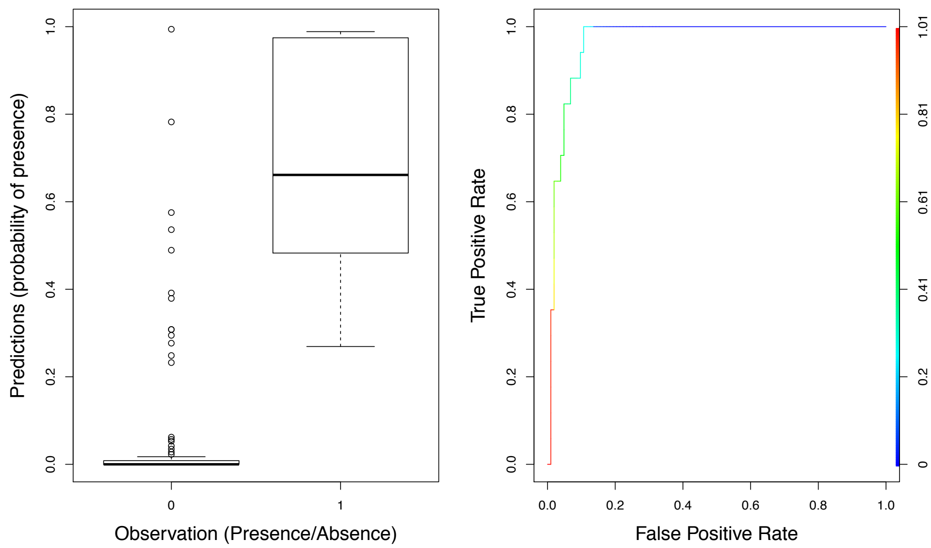

Figure A8: Accuracy of Random Forest (500 trees) fit against observed presence / absence of Rigid Gorgonians from 2010-2013 AUV surveys. Box plot of predicted probability of presence against observed presence (1) / absence (0) (left-hand panel). Receiver Operating Characteristic (ROC) curve characterising misclassification errors as a function of the probability threshold value chosen to discriminate between presence and absence (right-hand panel).

2.1.6 Random Forest model performance for Black Coral

Table A7: Confusion matrix with prediction error rates (top: false negatives; bottom: false positives) for the Random Forest distribution model (500 trees) for Black Coral .

Prediction	True	False	Error
0	110	5	0.043
1	0	5	1

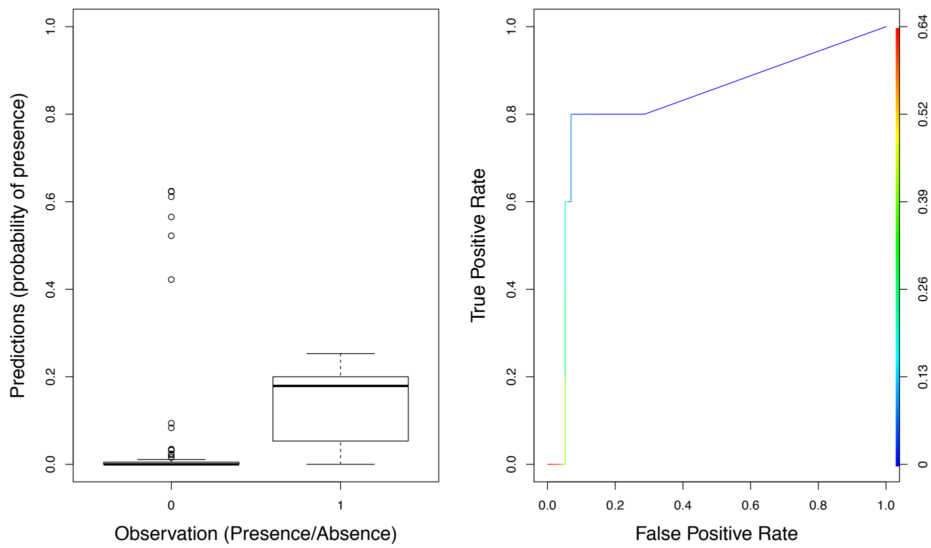

Figure A9: Accuracy of Random Forest (500 trees) fit against observed presence / absence of Black Coral from 2010-2013 AUV surveys. Box plot of predicted probability of presence against observed presence (1) / absence (0) (left-hand panel). Receiver Operating Characteristic (ROC) curve characterising misclassification errors as a function of the probability threshold value chosen to discriminate between presence and absence (right-hand panel).

2.1.7 Random Forest model performance for Branching Sponges

Table A8: Confusion matrix with prediction error rates (top: false negatives; bottom: false positives) for the Random Forest distribution model (500 trees) for Branching Sponges .

Prediction	True	False	Error
0	7	13	0.65
1	93	7	0.07

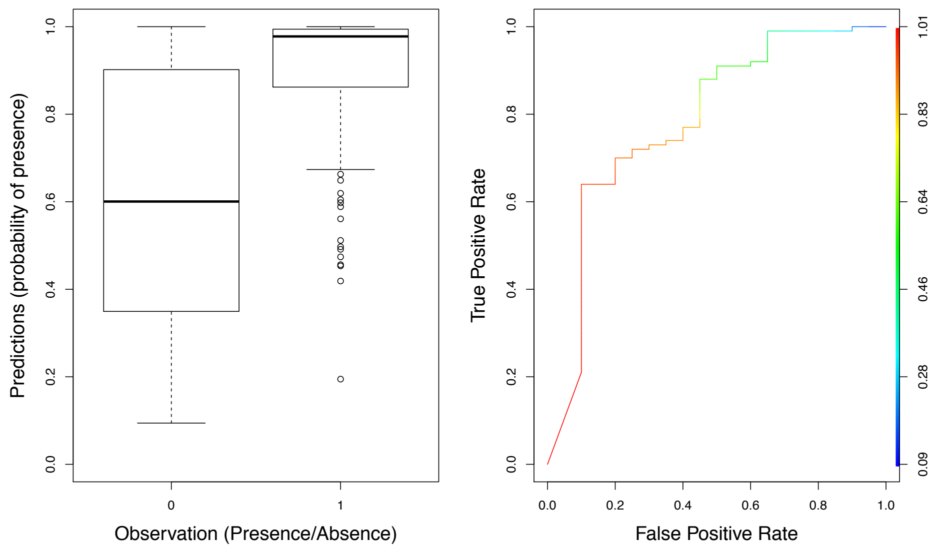

Figure A10: Accuracy of Random Forest (500 trees) fit against observed presence / absence of Branching Sponges from 2010-2013 AUV surveys. Box plot of predicted probability of presence against observed presence (1) / absence (0) (left-hand panel). Receiver Operating Characteristic (ROC) curve characterising misclassification errors as a function of the probability threshold value chosen to discriminate between presence and absence (right-hand panel).

2.1.8 Random Forest model performance for Laminar Sponges

Table A9: Confusion matrix with prediction error rates (top: false negatives; bottom: false positives) for the Random Forest distribution model (500 trees) for Laminar Sponges .

Prediction	True	False	Error
0	25	22	0.468
1	55	18	0.247

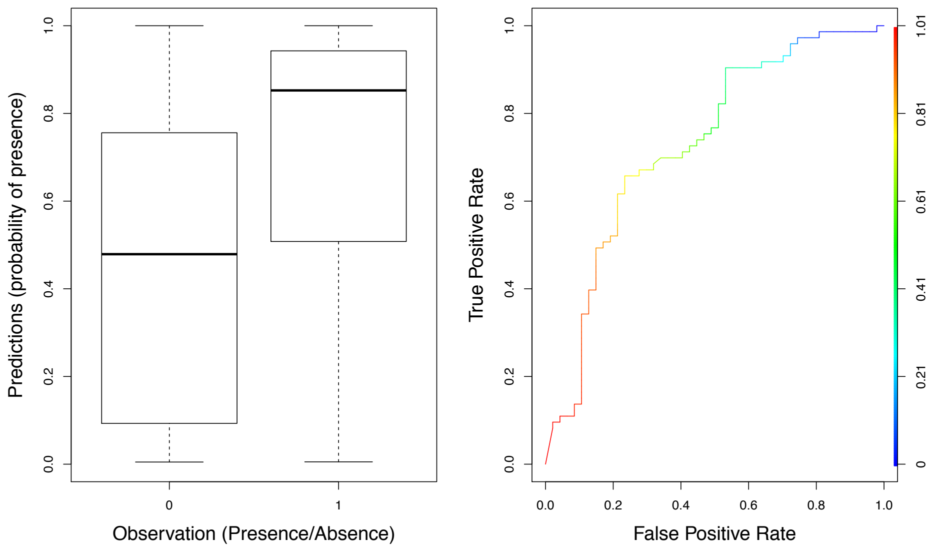

Figure A11: Accuracy of Random Forest (500 trees) fit against observed presence / absence of Laminar Sponges from 2010-2013 AUV surveys. Box plot of predicted probability of presence against observed presence (1) / absence (0) (left-hand panel). Receiver Operating Characteristic (ROC) curve characterising misclassification errors as a function of the probability threshold value chosen to discriminate between presence and absence (right-hand panel).

2.1.9 Random Forest model performance for Palmate Sponges

Table A10: Confusion matrix with prediction error rates (top: false negatives; bottom: false positives) for the Random Forest distribution model (500 trees) for Palmate Sponges .

Prediction	True	False	Error
0	64	12	0.158
1	26	18	0.409

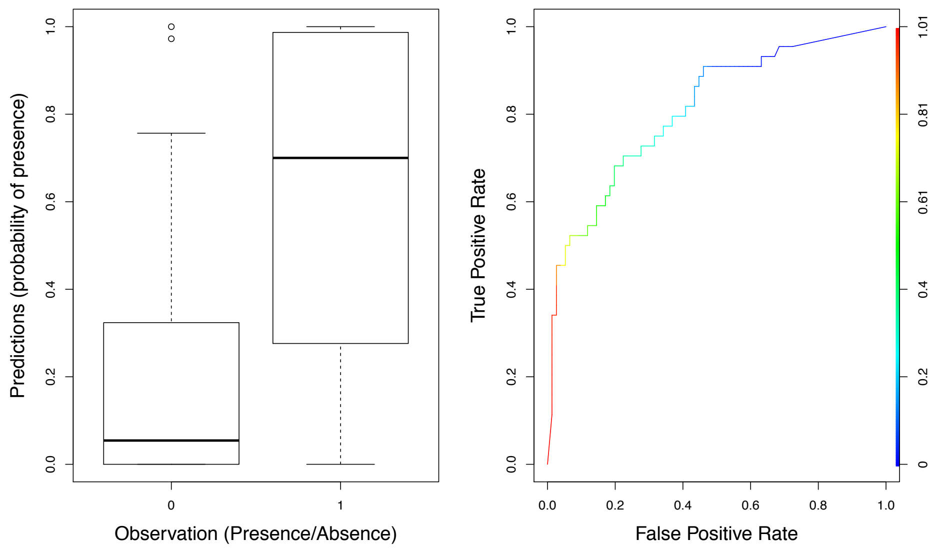

Figure A12: Accuracy of Random Forest (500 trees) fit against observed presence / absence of Palmate Sponges from 2010-2013 AUV surveys. Box plot of predicted probability of presence against observed presence (1) / absence (0) (left-hand panel). Receiver Operating Characteristic (ROC) curve characterising misclassification errors as a function of the probability threshold value chosen to discriminate between presence and absence (right-hand panel).

2.1.10 Random Forest model performance for Hollow Cup Sponges

Table A11: Confusion matrix with prediction error rates (top: false negatives; bottom: false positives) for the Random Forest distribution model (500 trees) for Hollow Cup Sponges .

Prediction	True	False	Error
0	6	12	0.667
1	97	5	0.049

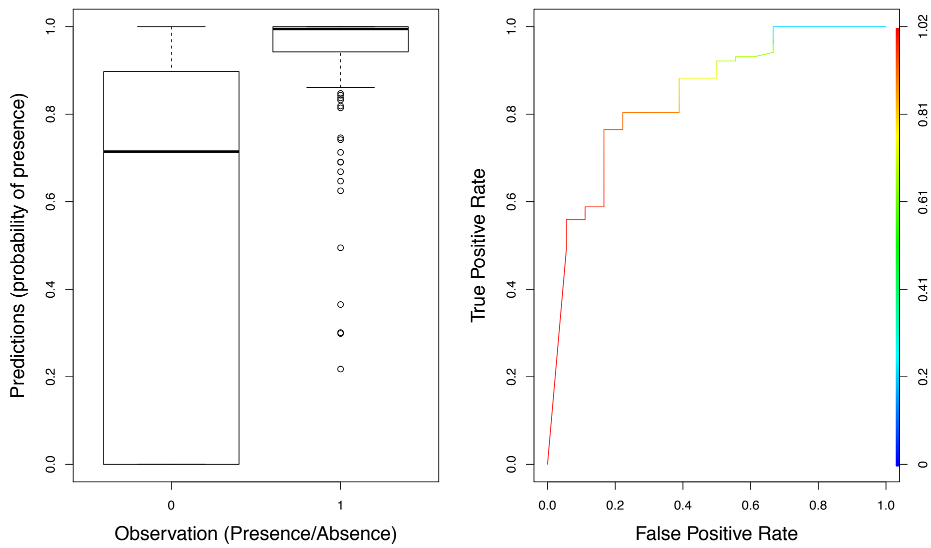

Figure A13: Accuracy of Random Forest (500 trees) fit against observed presence / absence of Hollow Cup Sponges from 2010-2013 AUV surveys. Box plot of predicted probability of presence against observed presence (1) / absence (0) (left-hand panel). Receiver Operating Characteristic (ROC) curve characterising misclassification errors as a function of the probability threshold value chosen to discriminate between presence and absence (right-hand panel).

2.1.11 Random Forest model performance for Hollow Tubular Sponges

Table A12: Confusion matrix with prediction error rates (top: false negatives; bottom: false positives) for the Random Forest distribution model (500 trees) for Hollow Tubular Sponges
.

Prediction	True	False	Error
0	93	9	0.088
1	3	15	0.833

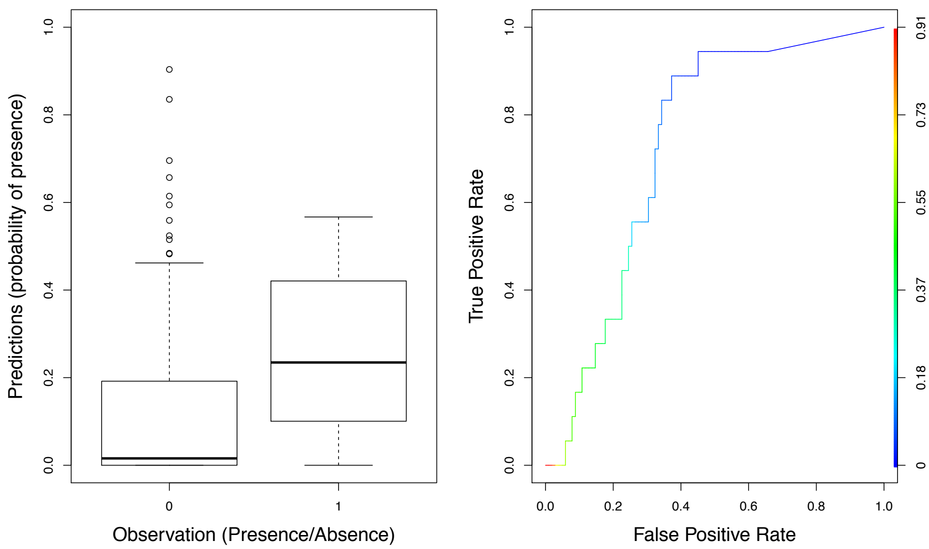

Figure A14: Accuracy of Random Forest (500 trees) fit against observed presence / absence of Hollow Tubular Sponges from 2010-2013 AUV surveys. Box plot of predicted probability of presence against observed presence (1) / absence (0) (left-hand panel). Receiver Operating Characteristic (ROC) curve characterising misclassification errors as a function of the probability threshold value chosen to discriminate between presence and absence (right-hand panel).

2.1.12 Random Forest model performance for Ball or Radiate Sponges

Table A13: Confusion matrix with prediction error rates (top: false negatives; bottom: false positives) for the Random Forest distribution model (500 trees) for Ball or Radiate Sponges .

Prediction	True	False	Error
0	76	9	0.106
1	28	7	0.2

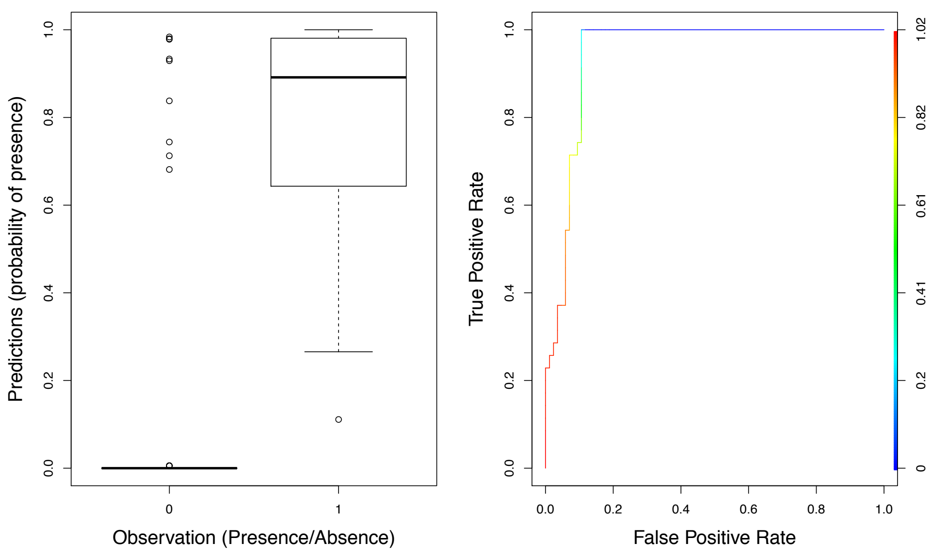

Figure A15: Accuracy of Random Forest (500 trees) fit against observed presence / absence of Ball or Radiate Sponges from 2010-2013 AUV surveys. Box plot of predicted probability of presence against observed presence (1) / absence (0) (left-hand panel). Receiver Operating Characteristic (ROC) curve characterising misclassification errors as a function of the probability threshold value chosen to discriminate between presence and absence (right-hand panel).

2.1.13 Random Forest model performance for Massive Form Sponges

Table A14: Confusion matrix with prediction error rates (top: false negatives; bottom: false positives) for the Random Forest distribution model (500 trees) for Massive Form Sponges .

Prediction	True	False	Error
0	68	8	0.105
1	36	8	0.182

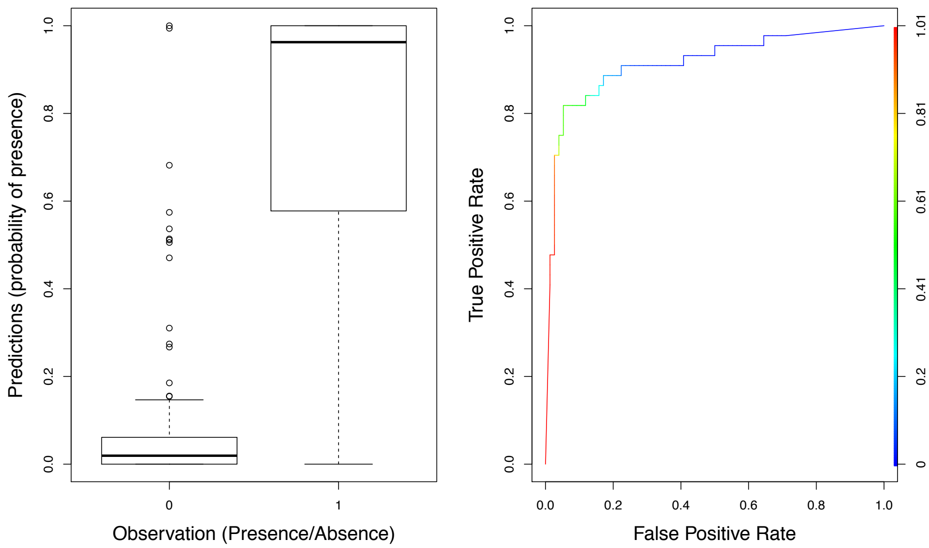

Figure A16: Accuracy of Random Forest (500 trees) fit against observed presence / absence of Massive Form Sponges from 2010-2013 AUV surveys. Box plot of predicted probability of presence against observed presence (1) / absence (0) (left-hand panel). Receiver Operating Characteristic (ROC) curve characterising misclassification errors as a function of the probability threshold value chosen to discriminate between presence and absence (right-hand panel).

3 Random Forest model spatial predictions of current, 2060s and change in group distribution

This section provides spatial predictions of current (2010s) and future (2060s) distribution for each functional group (Fig. A17). For each of the 13 groups, we present mapped predictions both in terms of probability of presence (top row) and presence/absence (bottom row). Note that presence/absence predictions were added during the review process to illustrate that changes in probability of presence translate as actual range extensions or contractions. Presence/absence estimates are however directly derived from Random Forests and correspond to the dominant mode across all classification trees, which is not always ecologically meaningful. Thus, binary presence/absence prediction maps would be more ecologically meaningful if model-specific threshold in the probability of presence were set to discriminate between presence or absence for each functional group.

(a) Stalked Solitary Ascidians

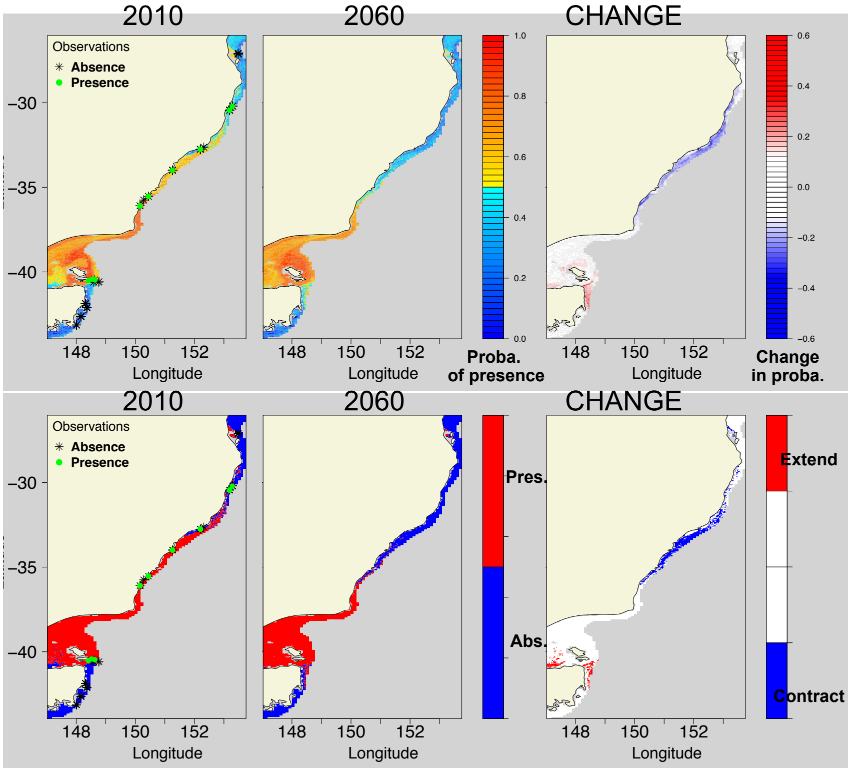

(b) Bryozoans

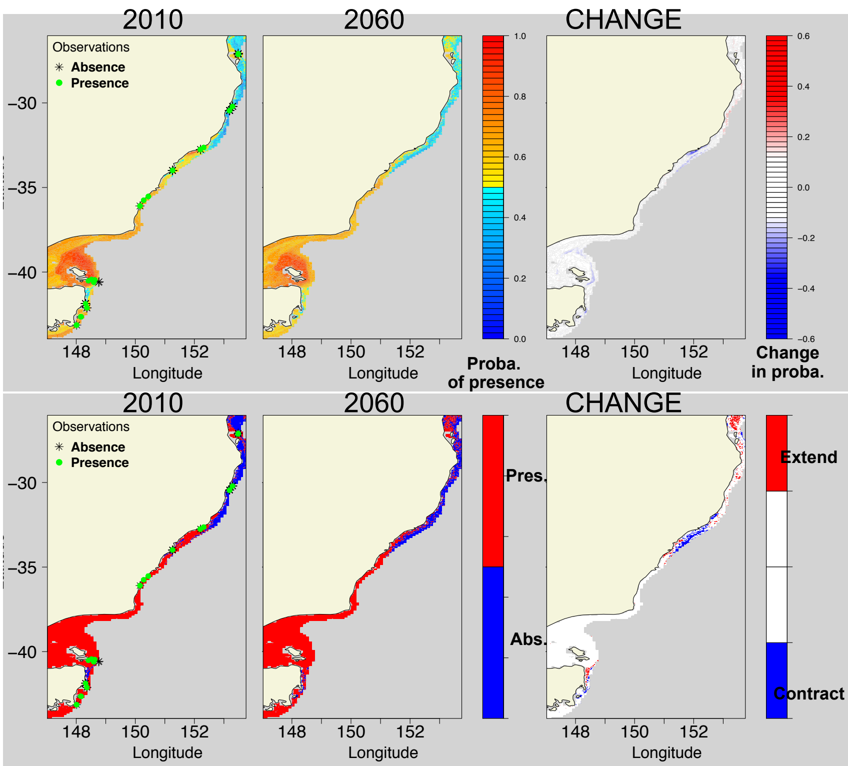

(c) Octocorals

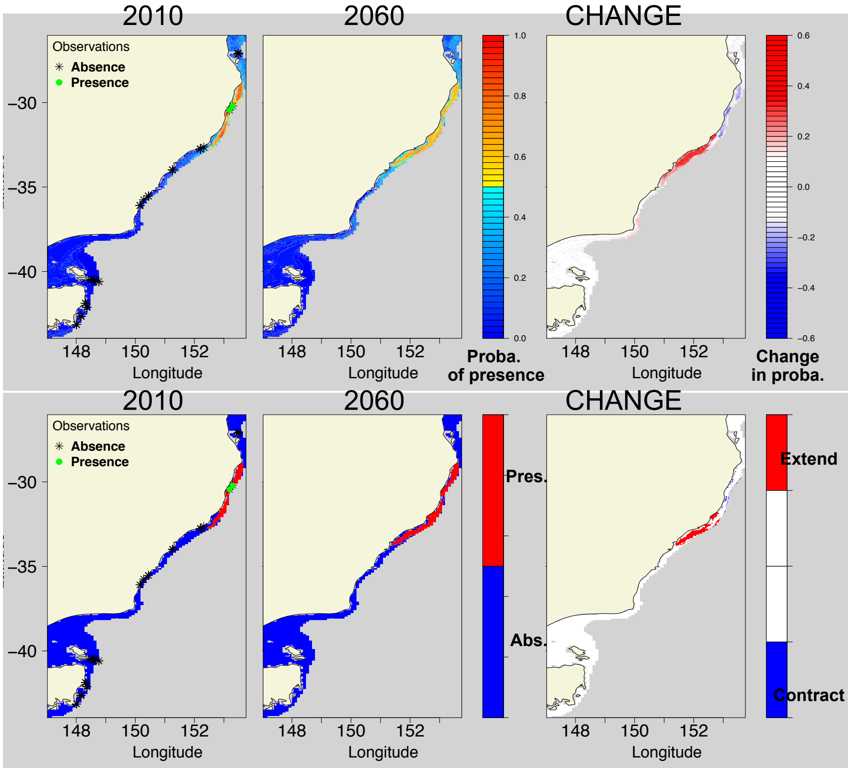

(d) Soft Gorgonians

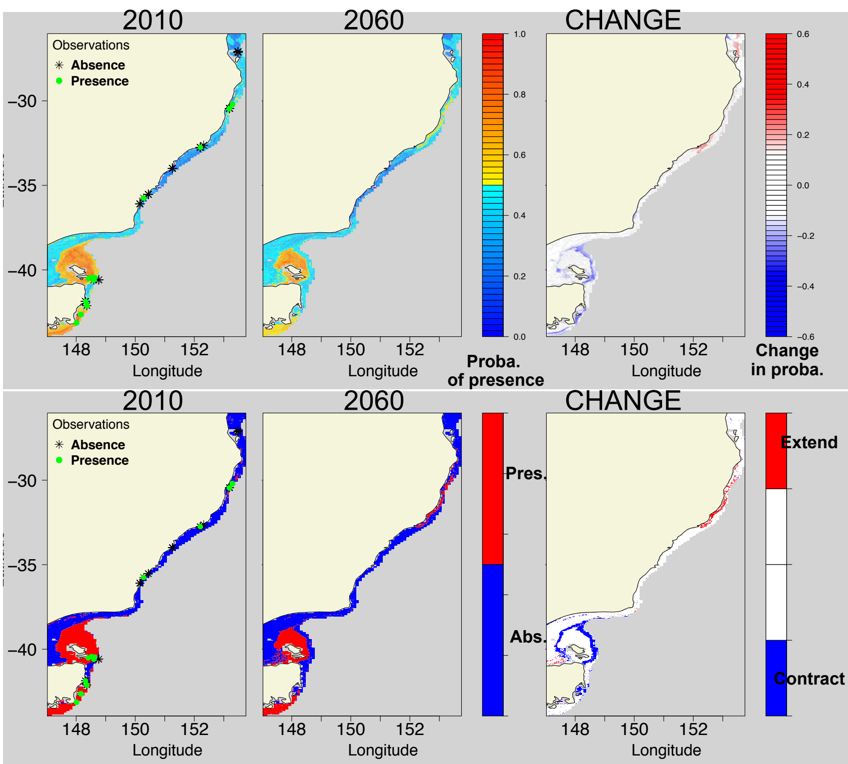

(e) Rigid Gorgonians

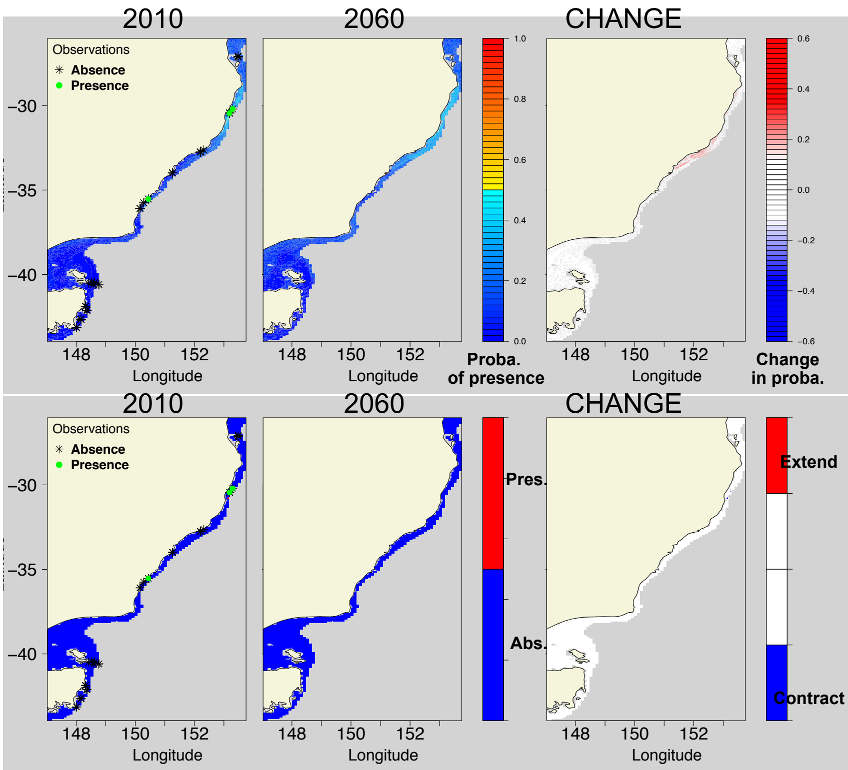

(f) Black Coral

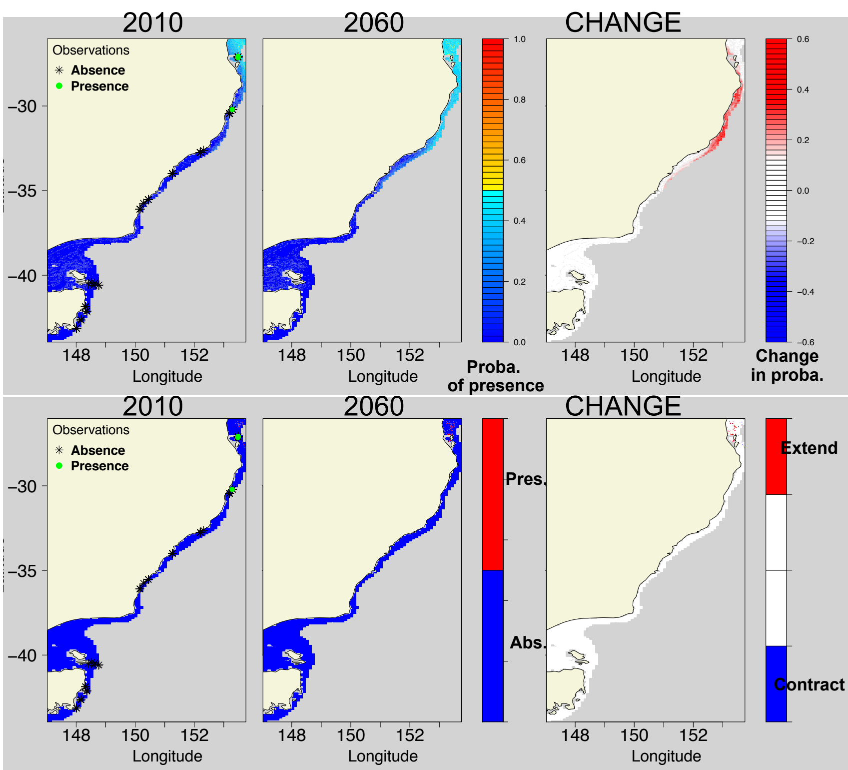

(g) Branching Sponges

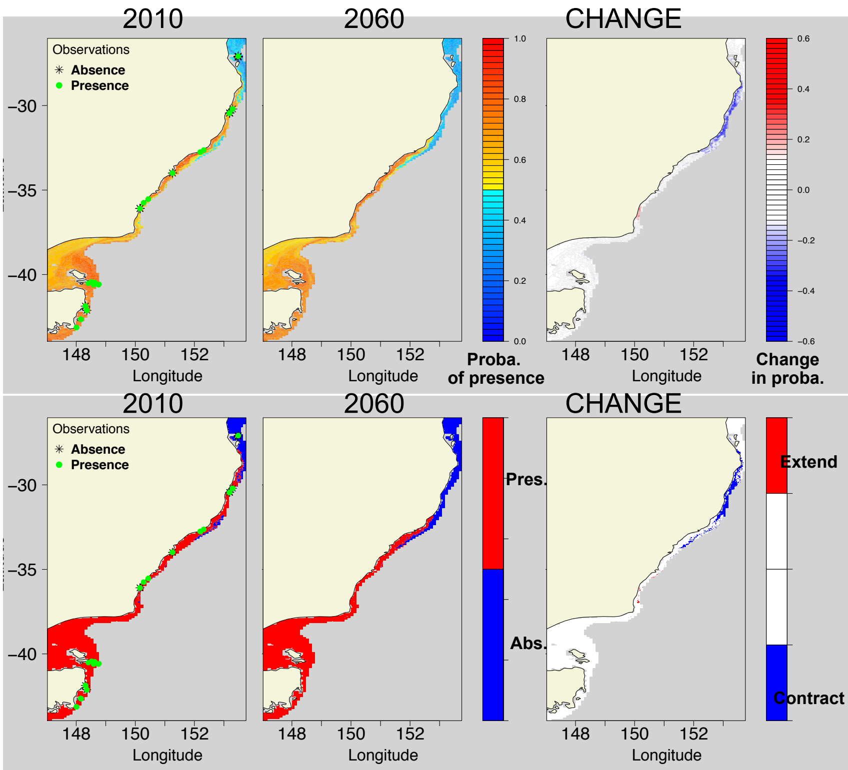

(h) Laminar Sponges

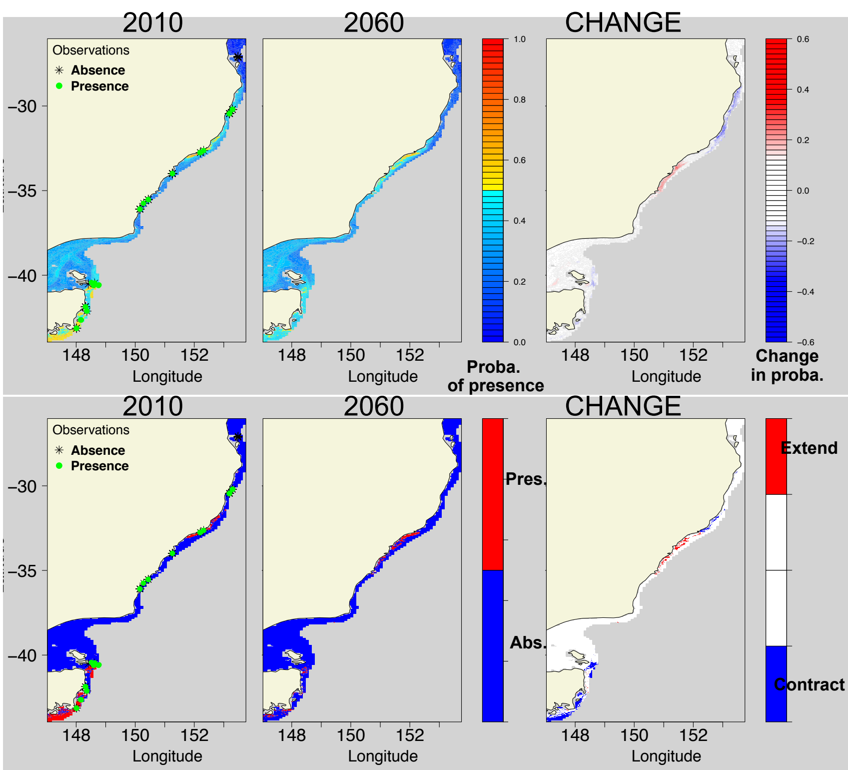

(i) Palmate Sponges

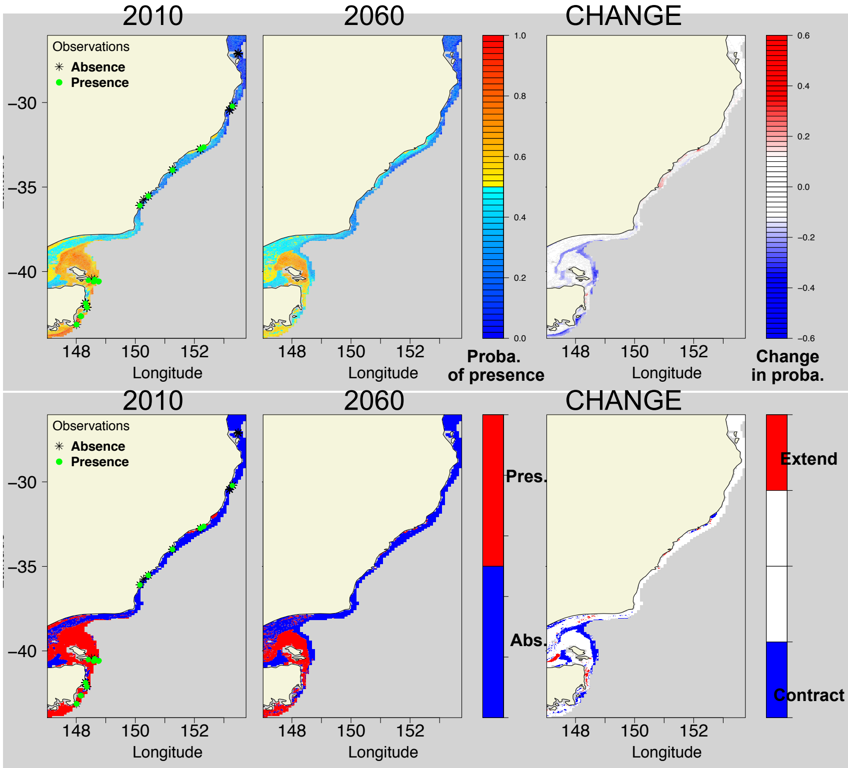

(j) Hollow Cup Sponges

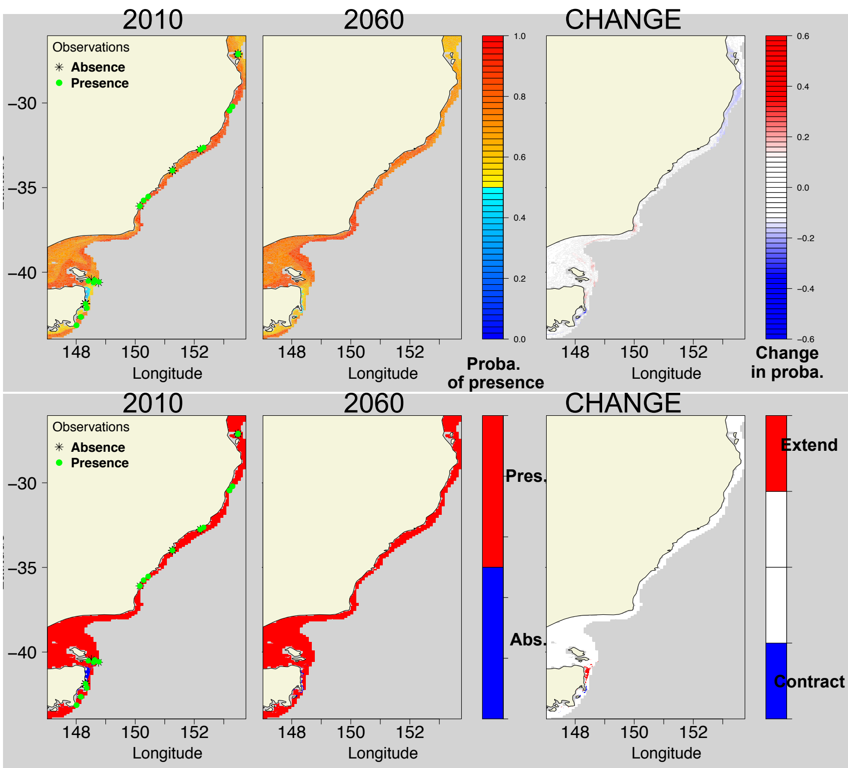

(k) Hollow Tubular Sponges

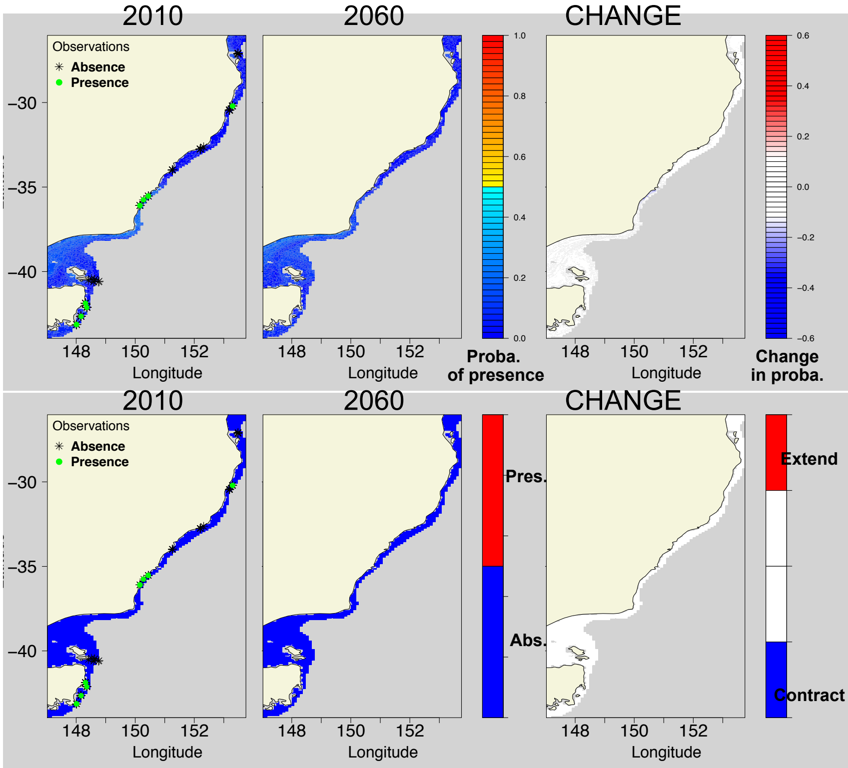

(l) Ball or Radiate Sponges

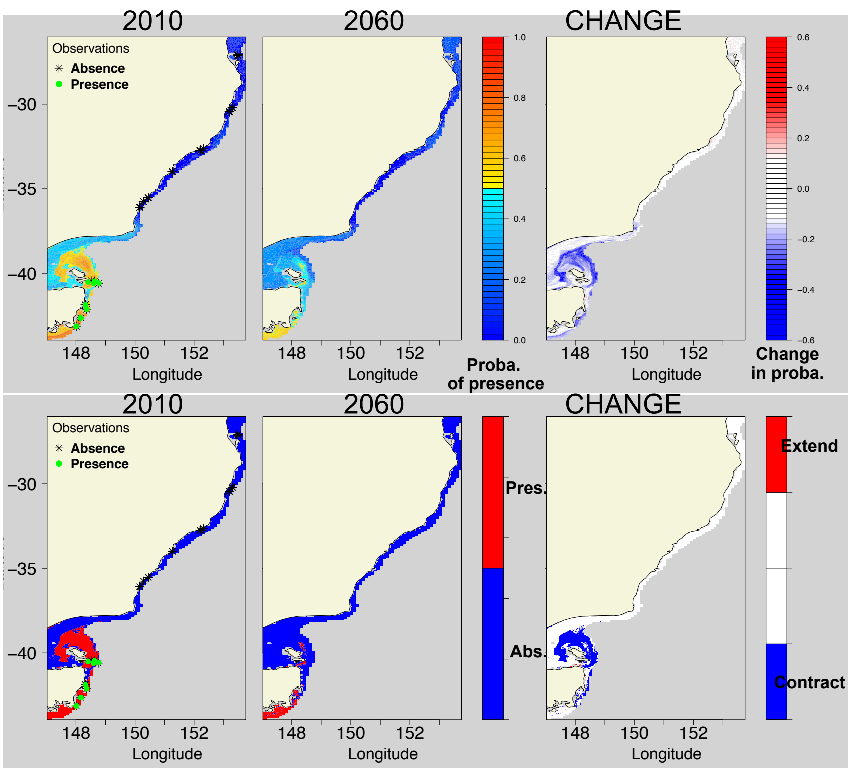

(m) Massive Form Sponges

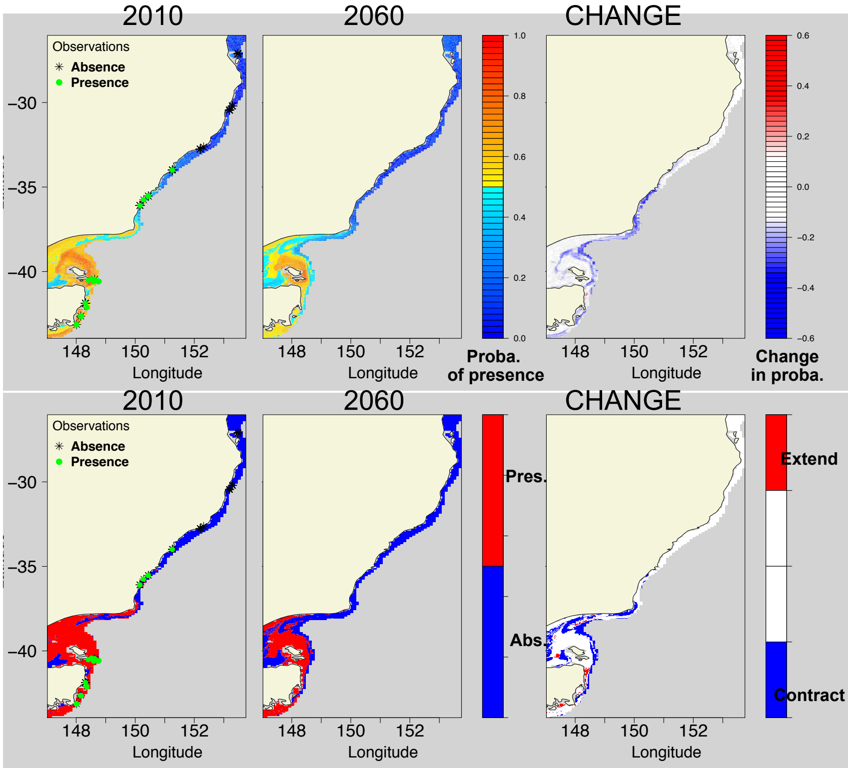

Figure A17: Predictions from Random Forest (500 trees) of current (left-hand panel), 2060s (centre panel) and relative change (right-hand panel) in the distribution of all 13 CATAMI groups. For each group (a to m), probability of presence and presence/absence estimates are given in the first and second row, respectively.

4 Projected changes in latitudinal distribution

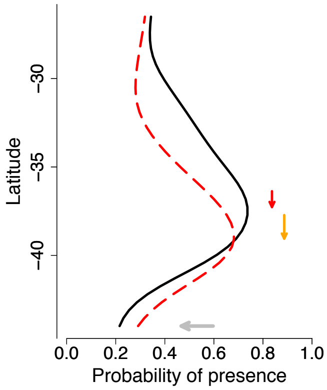

(a) Stalked Solitary Ascidians

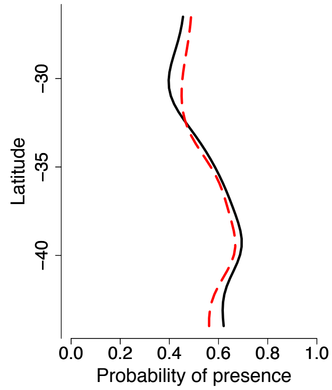

(b) Bryozoans

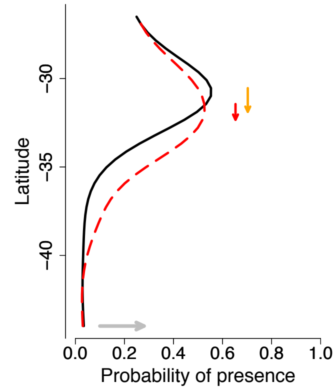

(c) Octocorals

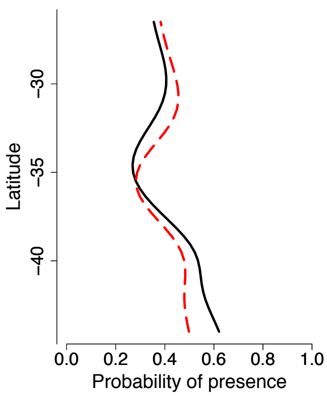

(d) Soft Gorgonians

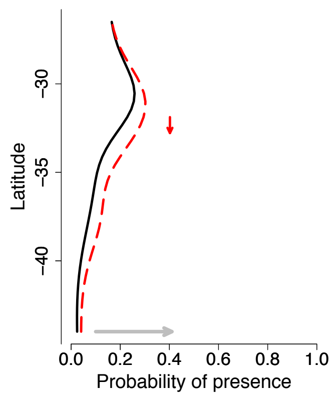

(e) Rigid Gorgonians

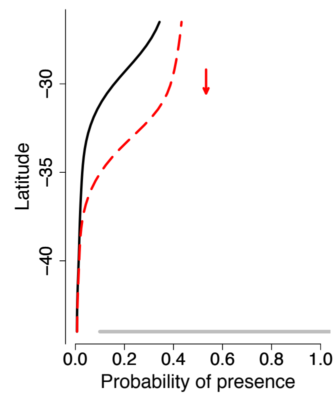

(f) Black Coral

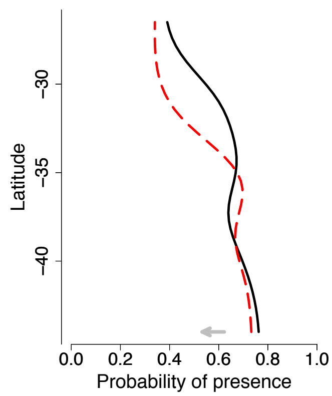

(g) Branching Sponges

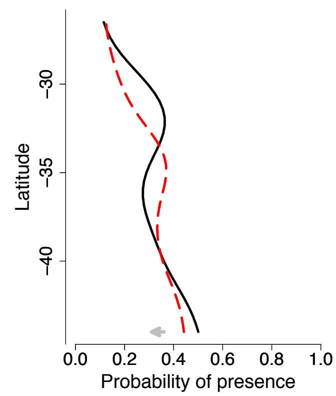

(h) Laminar Sponges

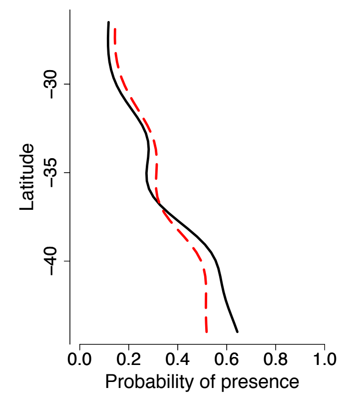

(i) Palmate Sponges

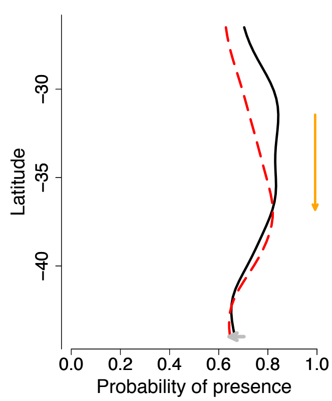

(j) Hollow Cup Sponges

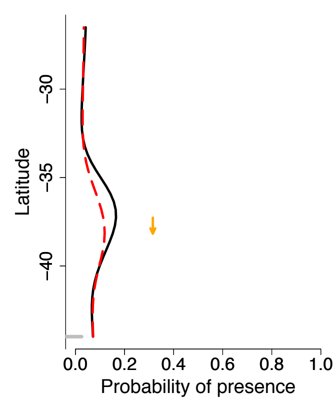

(k) Hollow Tubular Sponges

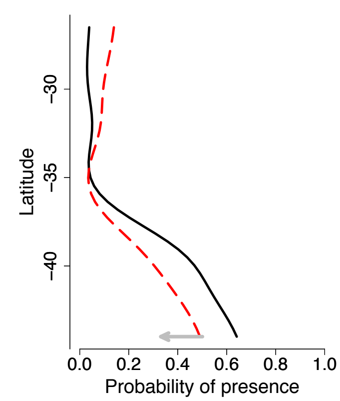

(l) Ball or Radiate Sponges

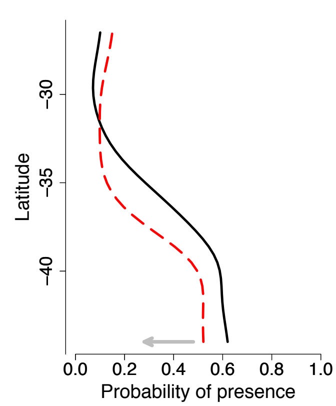

(m) Massive Form Sponges

Figure A18: Predictions from Random Forest (500 trees) of the current (black solid line) and 2060s (red dashed line) latitudinal distribution (i.e. predicted probability of presence) of 13 functional groups in eastern temperate Australia; Grey arrow reflects relative change in the probability of presence across the study region; Red and orange arrow symbolise latitudinal shifts in, respectively, the median and the maximum of the predicted probability of presence across the latitudinal gradient.

5 Additional contextual information: AUV dataset, strengths and limitations of the study

5.1 AUV dataset

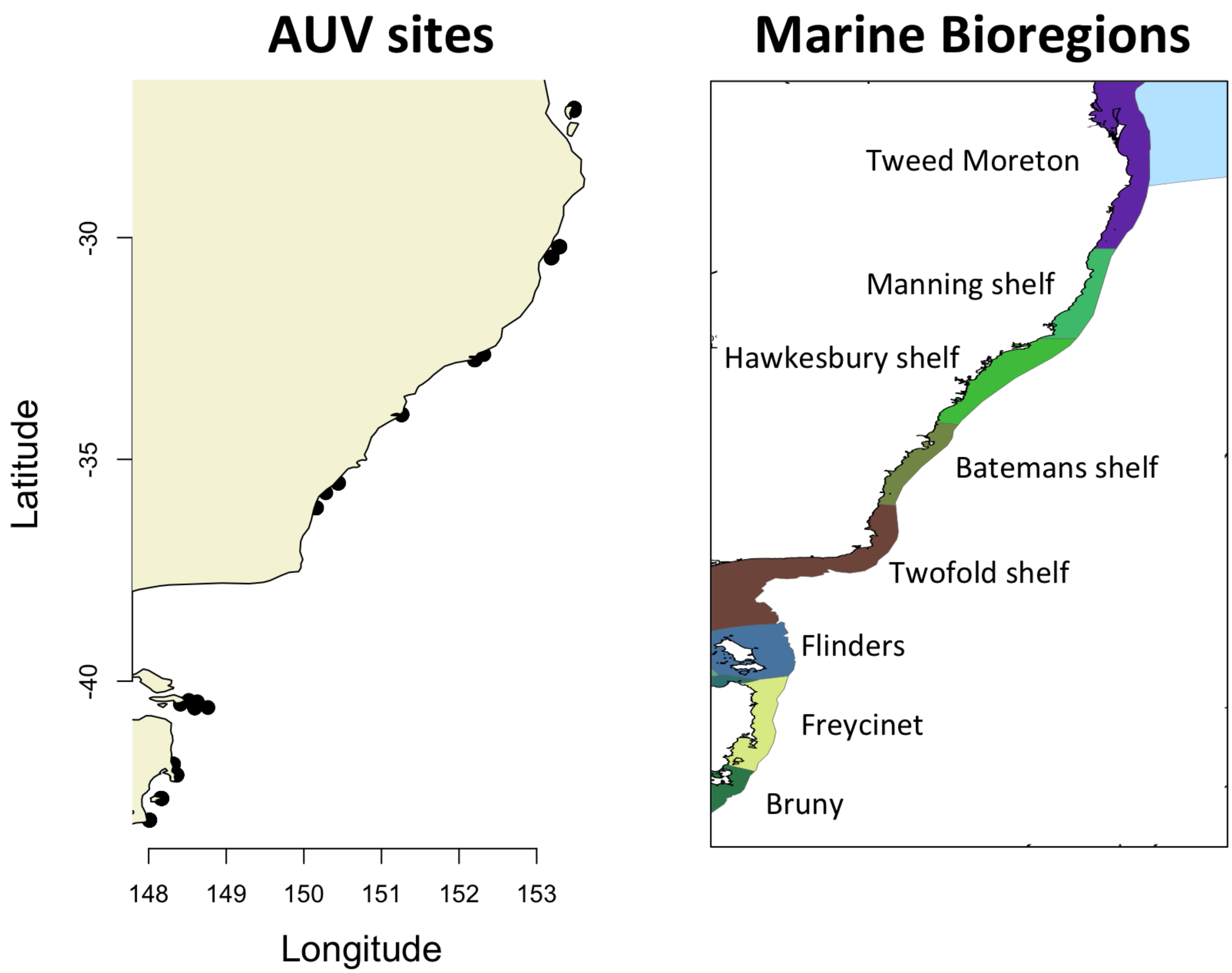

Figure A19: Maps of AUV survey sites (left-hand panel) and temperate Eastern and South-eastern Australia marine bioregions (right-hand panel; bioregion data available from the Australian Department of Environment and Energy). Note that 7 out of the 8 major marine bioregions are adequately sampled with the AUV surveys.

As specified in the paper, we used data from 120 independent AUV transects to train the model across 44 different survey sites and across large latitudinal and environmental gradients (e.g. depth, temperature, salinity... etc). James *et al.* (2017) [10] and the associated online appendix provide full details regarding the comprehensive hierarchical sampling by the AUV and the data used in our paper. To our knowledge, the size and nature of our data set is unprecedented for this kind of modelling ($\sim$ 1,800 images were analysed in detail, each corresponding to $\sim 2\text{m}^2$ of seafloor, with $>$ 10 images per transect, 3-5 transects per study site, and 3-5 sites in each of the 7 marine bioregions the surveys covered).

Given that the study region spans a broad latitudinal extent ($>$ 2,000 km north to south), the map provided in Fig. 1 only partially reflects the hierarchical structure and actual coverage of the AUV survey design. Survey sites that appear geographically close to each other on the map (Fig. 1; or left-hand panel of Fig. A19) may actually belong to distinct marine bioregions. For instance, the survey sites off the coast of Tasmania belong to 3 distinct bioregions, namely "Flinders" (northeast), "Freycinet" (central east) and "Bruny" bioregions (southeast) (see Fig. A19). Note also that all major marine bioregions (except for "Twofold Shelf" off the state of Victoria) were comprehensively surveyed along the subtropical to temperate coastlines of eastern Australia.

5.2 Strengths and Limitations of Presence/Absence distribution models

For reasons of simplicity and because of the nature of our imagery data over the large latitudinal gradient considered, we chose to use presence/absence models to characterise the biogeography of all groups and their broad responses to projected ocean changes. For all benthic groups with truncated latitudinal distributions (which are illustrated by the first 3 groups presented in Fig. 3), our dataset provides very reliable estimates of "true/functional" absences across the large latitudinal gradient. For instance, AUV surveys gives us confidence that no cold temperate sponges occur at ecologically significant levels north of northern New-South-Wales, and conversely that subtropical groups do not currently occur in southeastern Australia. In this sense, our dataset is well suited to characterise the broad environmental niches of the different groups considered. Note also that, as mentioned in the online-only Methods section, we did compare alternative statistical methods (i.e. GLMs - Generalised Linear Models - and GAMs - Generalised Additive Models) that led to similar predictions, but we only present results from the random forests for simplicity and because they performed better overall.

While we do not predict abundance or percentage cover, projected changes in probability of presence most certainly reflect significant range contractions and extensions in the occurrence of the different groups as demonstrated with the binary presence/absence maps (Fig. A17). Thus, while the predicted changes in community structure are based on presence/absence models, they most likely translate into significant changes in diversity (functional richness) and community composition. It is the broad range shifts of region-specific groups across several degrees of latitude that underpins the predicted changes in community structure by 2060, and we have no reason to believe these predictions are unreliable. For example, the predicted decay of cold temperate species from the study area by 2060 (except for the south coast of Tasmania) is entirely consistent with present day distributions relative to environmental variables, and we would not expect this result to be any different were it analysed in terms of relative abundance or percentage cover. We recognise that our models have limited abilities to finely predict the current distribution of broadly-distributed functional groups and expected (marginal) changes in the distributions of these groups by 2060. But, again, note that our predictions of changes in community structure are largely driven by changes in the distributions of region-specific groups (Fig. 3 and 4), for which model predictions have high accuracy.

5.3 Strengths and Limitations of predicted latitudinal range shifts

Our spatial predictions explicitly account for depth within the 30-90 m mesophotic range surveyed by the AUV. Depth is transect-specific in the data and constitutes an important environmental covariate to predict the occurrence of a number of groups (Fig. 2). However, our predictions of vertical shifts are constrained by the data used to fit the models, and hence are restricted to the depth range where each functional group was observed in the AUV surveys. Thus, we discuss model predictions mostly in terms of latitudinal ranges given that projections of regional ocean changes (mostly related to increased southwards penetration of the East Australian Current) are fairly homogeneous on the continental shelf across depth so the main patterns of predicted change occur across latitudes.

We acknowledge that, at a given latitude, in a regionally warmer future, some of the functional groups we considered may shift their depth range to depths greater than that which we considered in this study. However, that does not detract from the important result of expected latitudinal range shifts within the depth range of our study. It is also worth noting that no broad-scale information is currently available about the occurrence of the different functional groups at depths greater than 90 m, and that knowledge of fine-scale depth-dependent near-bottom environmental conditions is limited. Thus, characterising local changes in the depth distribution of functional groups will require dedicated research in the future. Note, however that we are confident in our results concerning broad-scale changes in the biogeography of the different groups because our predictions importantly capture the main effect of global change in the region, i.e. large-scale climate-driven ocean changes due to the increased southwards penetration of the warm nutrient-poor East Australian Current.

References

[1] Huang, Z. Bathymetry derived topographic relief grid. Tech. Rep., Geoscience Australia, Canberra (2013).

[2] Chamberlain, M. A., Sun, C., Matear, R. J., Feng, M. & Phipps, S. J. Downscaling the climate change for oceans around australia. *Geoscientific Model Development* **5**, 1177–1194 (2012). URL http://www.geosci-model-dev.net/5/1177/2012/.

[3] Sun, C. *et al.* Marine downscaling of a future climate scenario for australian boundary currents. *Journal of Climate* **25**, 2947–2962 (2012). URL http://dx.doi.org/10.1175/JCLI-D-11-00159.1. http://dx.doi.org/10.1175/JCLI-D-11-00159.1.

[4] Matear, R. J., Chamberlain, M. A., Sun, C. & Feng, M. Climate change projection of the tasman sea from an eddy-resolving ocean model. *Journal of Geophysical Research: Oceans* **118**, 2961–2976 (2013). URL http://dx.doi.org/10.1002/jgrc.20202.

[5] Smale, D. A. & Wernberg, T. Satellite-derived sst data as a proxy for water temperature in nearshore benthic ecology. *Marine Ecology Progress Series* **387**, 27–37 (2009). URL http://www.int-res.com/abstracts/meps/v387/p27-37/.

[6] Stobart, B., Mayfield, S., Mundy, C., Hobday, A. J. & Hartog, J. R. Comparison of in situ and satellite sea surface-temperature data from south australia and tasmania: how reliable are satellite data as a proxy for coastal temperatures in temperate southern australia? *Marine and Freshwater Research* **67**, 612–625 (2016). URL http://www.publish.csiro.au/paper/MF14340.

[7] Oliver, E. C. J. & Holbrook, N. J. A statistical method for improving continental shelf and nearshore marine climate predictions. *Journal of Atmospheric and Oceanic Technology* **31**, 216–232 (2014). URL http://dx.doi.org/10.1175/JTECH-D-13-00052.1.

[8] Oliver, E. C. J. & Holbrook, N. J. Extending our understanding of south pacific gyre spin-up: Modeling the east australian current in a future climate. *Journal of Geophysical Research: Oceans* **119**, 2788–2805 (2014). URL http://dx.doi.org/10.1002/2013JC009591.

[9] Breiman, L. Random forests. *Machine Learning* **45**, 5–32 (2001). URL http://dx.doi.org/10.1023/A%3A1010933404324.

[10] James, L. C., Marzloff, M. P., Barrett, N., Friedman, A. & Johnson, C. R. Changes in deep reef benthic community composition across a latitudinal and environmental gradient in temperate eastern australia. *Marine Ecology Progress Series* **565**, 35–52 (2017). URL http://www.int-res.com/abstracts/meps/v565/p35-52/.